Purinergic Signalling (2014) 10:291–304
DOI 10.1007/s11302-013-9388-x

ORIGINAL ARTICLE

Loss of P2X7 nucleotide receptor function leads to abnormal fat distribution in mice

Kim L. Beaucage · Andrew Xiao · Steven I. Pollmann · Matthew W. Grol · Ryan J. Beach · David W. Holdsworth · Stephen M. Sims · Mark R. Darling · S. Jeffrey Dixon

Received: 3 May 2013 / Accepted: 10 September 2013 / Published online: 13 November 2013

Abstract The P2X7 receptor is an ATP-gated cation channel expressed by a number of cell types. We have shown previously that disruption of P2X7 receptor function results in downregulation of osteogenic markers and upregulation of adipogenic markers in calvarial cell cultures. In the present study, we assessed whether loss of P2X7 receptor function results in changes to adipocyte distribution and lipid accumulation in vivo. Male P2X7 loss-of-function (KO) mice exhibited significantly greater body weight and epididymal fat pad mass than wild-type (WT) mice at 9 months of age. Fat pad adipocytes did not differ in size, consistent with adipocyte hyperplasia rather than hypertrophy. Histological examination revealed ectopic lipid accumulation in the form of adipocytes and/or lipid droplets in several non-adipose tissues of older male KO mice (9–12 months of age). Ectopic lipid was observed in kidney, extraorbital lacrimal gland and pancreas, but not in liver, heart or skeletal muscle. Specifically, lacrimal gland and pancreas from 12-month-old male KO mice had greater numbers of adipocytes in perivascular, periductal and acinar regions. As well, lipid droplets accumulated in the renal tubular epithelium and lacrimal acinar cells. Blood plasma analyses revealed diminished total cholesterol levels in 9- and 12-month-old male KO mice compared with WT controls. Interestingly, no differences were observed in female mice. Moreover, there were no significant differences in food consumption between male KO and WT mice. Taken together, these data establish novel in vivo roles for the P2X7 receptor in regulating adipogenesis and lipid metabolism in an age- and sex-dependent manner.

Keywords Adipocyte · Cholesterol · Exocrine · Kidney · Metabolic syndrome · *P2rx7*

Introduction

Global epidemics of metabolic syndrome diseases represent major health and economic burdens, with incidences on the rise [1, 2]. Obesity (central adiposity), dyslipidemia, hypertension, type 2 diabetes mellitus and cardiovascular diseases are hallmarks of metabolic syndrome [3]. Recent studies have shown that, in addition to lipid storage, adipose tissue regulates other tissues and systems throughout the body. In particular, adipose is an active endocrine organ [2, 4] that is involved in cross-talk with other tissue types such as bone [5, 6]. Moreover, it plays important roles in local and systemic inflammation [7, 8] and energy metabolism [9–11].

Extracellular nucleotides, such as ATP, signal through purinergic (P2) receptors on the membrane of most cell types. Two subfamilies of P2 receptors exist: P2X (ATP-gated nonselective cation channels) and P2Y (G protein-coupled receptors) [12]. There are seven subtypes of P2X receptors, P2X1–7. P2X7 is of emerging interest as a potential

Electronic supplementary material The online version of this article (doi:10.1007/s11302-013-9388-x) contains supplementary material, which is available to authorized users.

K. L. Beaucage · A. Xiao · R. J. Beach · S. M. Sims · S. J. Dixon (✉)
Department of Physiology and Pharmacology, The University of Western Ontario, London, ON, Canada N6A 5C1
e-mail: jeff.dixon@schulich.uwo.ca

S. I. Pollmann · D. W. Holdsworth
Robarts Research Institute, The University of Western Ontario, London, ON, Canada N6A 5C1

M. W. Grol
Department of Anatomy and Cell Biology, The University of Western Ontario, London, ON, Canada N6A 5C1

M. R. Darling
Department of Pathology, The University of Western Ontario, London, ON, Canada N6A 5C1

therapeutic target in a number of diseases. This receptor is unique in that it is activated by relatively high concentrations of ATP. Moreover, P2X7 signaling can cause the formation of large nonselective membrane pores and induce dynamic membrane blebbing [12, 13]. This receptor plays important roles in chronic pain [14, 15], apoptosis [16–18], bone remodeling [19–21], immune responses [22–25] and the function of exocrine and endocrine organs [26, 27].

Genetically modified mice that lack functional P2X7 receptors (KO mice) present with an osteopenic phenotype owing to diminished periosteal bone formation and excessive trabecular bone resorption [19]. Moreover, these mice exhibit an impaired skeletal response to mechanical loading [20]. In vitro evidence has since demonstrated that activation of P2X7 receptors in bone-forming osteoblasts results in cell-autonomous enhancement of differentiation and matrix mineralisation [13]. In addition, cultures of bone cells from P2X7 KO mice, which include mesenchymal progenitors, display greater expression of adipogenic markers compared with cultures from wild-type (WT) mice. This upregulation of adipogenic markers was accompanied by downregulation of osteogenic markers and suppression of osteoblastic differentiation [13]. Osteoblasts and adipocytes both arise from mesenchymal stem cells and become terminally differentiated through expression of master transcription factors such as Runx2 and peroxisome proliferator-activated receptor γ [28–30]. Therefore, evidence points to P2X7 playing a critical role in directing differentiation toward the osteoblast lineage and away from the adipocyte lineage.

The P2X7 receptor has also been shown to regulate cellular metabolism. Activation of P2X7 on osteoblast-like cells dramatically increases the production of metabolic acid [31]. This P2X7-induced increase in proton efflux is dependent on the activity of phosphatidylinositol 3-kinase and the presence of glucose. It has also been shown that heterologous expression of P2X7 in HEK293 cells promotes aerobic glycolysis and increases levels of glycolytic enzymes and glycogen stores [32]. Therefore, P2X7 activation enhances cellular energy metabolism, suggesting a role for this receptor in energy homeostasis.

Expression of functional P2X7 receptors has been reported in adipocytes purified from murine white adipose tissue [33], as well as cultured adipocytes from human visceral and subcutaneous adipose tissues [34]. However, little is known about the role of P2X7 receptors in adipose tissue. Recent studies have reported that ablation of *P2rx7*, the gene encoding P2X7, does not affect body and gonadal fat pad weights in mice up to 4 months of age [33]. In the present study, we report that loss of P2X7 function leads to increased adiposity and lipid accumulation in older male mice. P2X7 KO mice were found to have increased body and epididymal fat pad weights and reduced total plasma cholesterol levels compared with WT mice at 9 months of age. Ectopic lipid deposits were observed in the kidneys, pancreas and extraorbital lacrimal glands. There were no significant differences in food consumption by KO and WT mice at any age. These results point to heretofore unrecognised roles for the P2X7 receptor in adipogenesis and lipid metabolism.

Materials and methods

Animals

The P2X7 KO mouse was obtained from Pfizer [25]. To generate this mouse, the *P2rx7* gene was modified by a deletion followed by insertion of a neomycin cassette in exon 13, leading to disruption of the carboxyl-terminal coding region [25, 35]. Several studies have confirmed that there is no detectable P2X7 function in cells isolated from this KO mouse. For example, in contrast to WT cells, peritoneal macrophages from the KO mouse do not exhibit pore formation in response to high concentrations of ATP [25, 36]. Similarly, calvarial osteoblasts from WT, but not KO mice, exhibit pore formation [19] and membrane blebbing [37] in response to the P2X7 agonist 2′(3′)-*O*-(4-benzoylbenzoyl)ATP (BzATP). Moreover, BzATP and high concentrations of ATP induce a slowly deactivating inward current in osteoclasts from WT but not KO mice [19]. The current–voltage relationship of this conductance is consistent with that reported for P2X7 current in rabbit osteoclasts [38]. Although a splice variant (with C-terminal truncation) has been detected in some tissues of the Pfizer KO mouse, it is inefficiently trafficked to the cell surface and displays greatly diminished receptor function [39]. Thus, there appears to be global loss of P2X7 function in the Pfizer KO mouse model.

In the present study, mice were maintained on a mixed genetic background (129/Ola × C57BL/6 × DBA/2) by cross-breeding of heterozygous mice. Genotypes were identified by polymerase chain reaction (PCR). Mice were housed in standard cages and maintained on a 12-h light/dark cycle, with water and standard mouse chow (2018 Teklad Global 18 % protein rodent diet, Harlan Laboratories, Indianapolis, IN, USA) available ad libitum. All aspects of this study were conducted in accordance with the policies and guidelines of the Canadian Council on Animal Care and were approved by the Animal Use Subcommittee of the University of Western Ontario, London, ON, Canada.

Food intake and body composition of 2-, 6-, 9- and 12-month-old WT and KO mice were assessed. For these studies, mice were housed individually. Mice and food were weighed using a portable electronic scale (Acculab VICON VIC-511; Sartorius Group, Goettingen, Germany). Food intake was determined by subtracting the weight of food remaining after each week from the initial amount of food provided.

Micro-computed tomography (micro-CT)

Mice were anesthetised with isoflurane (Forane, catalog # CA2L9100, Baxter Corporation, Mississauga, ON, Canada) and imaged using an eXplore Locus Ultra Micro-computed tomography (micro-CT) scanner or an eXplore speCZT scanner (GE Healthcare Biosciences, London, ON, Canada). Scans were analysed as described previously [40]. Briefly, a calibrating phantom composed of air, water and cortical bone-mimicking epoxy (SB3; Gammex, Middleton WI, USA) [41] was scanned together with the animals. On the eXplore Locus Ultra, 1,000 projection images were obtained over a single 16-s rotation (80 kVp, 55 mA tube current, 16 ms exposure). On the speCZT scanner, 900 projection images were obtained over a single 5-min rotation (90 kVp, 40 mA tube current, 16 ms exposure). Each of the eXplore Locus Ultra and speCZT data sets were reconstructed into 3D volumes with an isotropic voxel spacing of 154 and 150 μm, respectively, and scaled into Hounsfield units (HU). Using MicroView software (GE Healthcare Biosciences), three signal-intensity thresholds (−200, −30 and 190 HU) were used to classify each voxel as adipose, lean or skeletal tissue, respectively. Custom software was used to calculate tissue masses from assumed tissue densities of 0.95 (adipose), 1.05 (lean) and 1.92 (skeletal) g/cm^3. The computed total mass corresponded well with the measured weight of each mouse (within 3 %). In addition, the software was used to calculate bone mineral density (BMD) and bone mineral content (BMC). Briefly, BMD was obtained as the ratio of the average HU value of the skeletal region of interest to the measured HU value of the SB3 calibrator, multiplied by the known hydroxyapatite-equivalent density of the SB3 (1.1 g/cm^3). Thereafter, the program automatically computed BMC as the product of the BMD and the total volume of the skeletal region of interest used in the BMD calculation.

Histology and histomorphometry

Mice were fasted 6 h prior to euthanasia by CO_2 (100 %) asphyxiation. Mice were weighed and organs harvested, weighed and prepared for histological analyses using standard protocols. The following organs/tissues were examined: epididymal/retroperitoneal fat pads, heart, liver, spleen, pancreas, kidneys, salivary glands (submandibular and sublingual), extraorbital lacrimal glands, Harderian glands and skeletal muscle (quadriceps). All tissues were fixed in 10 % neutral buffered formalin (pH 7.0). Some samples were then processed, paraffin-embedded and blocks were sectioned at 5 μm thickness using a Leica RM2255 microtome (Leica Microsystems, Wetzlar, Germany). Sections were mounted on positively charged glass slides (Superfrost plus microslides; VWR International, Mississauga, ON, Canada) and stained with haematoxylin and eosin (H&E, Harris hematoxylin and eosin; Surgipath, Leica Microsystems).

Adipocyte number and diameter in fat pads were determined using Image Master software (Photon Technology International Inc., London, ON, Canada). Adipocyte density was calculated as the number of adipocytes within the field of view (FOV) divided by the area of the FOV (1.30 mm^2). Adipocyte diameter was obtained by measuring the maximum diameter of each adipocyte within the same FOV.

After harvest, other samples were manually cut into small (2×2×2 mm) portions in preparation for staining with osmium tetroxide (modified from [42]) to reveal lipid deposits. Briefly, tissue samples were fixed in 10 % neutral buffered formalin (pH 7.0) overnight, washed and stained with osmium tetroxide (VWR International) 1 % in water for 2 h with intermittent agitation. Samples were then washed with water for 15 min×2, differentiated with 5 % periodic acid solution in water (Alfa Aesar, Ward Hill, MA, USA) for 30 min, agitating periodically and washed twice more with running water for 30 min each. Samples were then processed, paraffin-embedded, sectioned and stained with H&E.

Osmium tetroxide staining was quantified using a Leica DM1000 microscope coupled to a DFC295 digital camera and Leica Application Suite software (version 3.8.0). Brightness and contrast were adjusted by the same amounts for all images of each tissue type (both WT and KO). A blinded observer then quantified the area of tissue stained with osmium tetroxide using Image Master software. For all images of each tissue, brightness and threshold values for the RGB channels were adjusted to select for osmium tetroxide staining (black), but not haematoxylin or eosin staining. To quantify total tissue area, brightness and RGB thresholds were adjusted to select for the total area of stained tissue (including osmium tetroxide, haematoxylin and eosin). The area of osmium-positive staining was reported as a percentage of total tissue area.

Blood plasma chemistry and tissue lipid analyses

Mice were fasted for 6 h prior to euthanasia by CO_2 asphyxiation. Cardiac puncture was performed immediately post-mortem to obtain plasma samples for analysis of glucose, triglyceride and total cholesterol levels. Blood, treated with EDTA anticoagulant, was sedimented for 10 min at 10,000 rpm. Plasma was stored frozen at −20 °C, and contents were analyzed using a Cobas Mira S autoanalyser (Metabolic Phenotyping Laboratory, Robarts Research Institute, London, ON, Canada). In addition, immediately following cardiac puncture, some tissues were harvested, snap-frozen in liquid nitrogen and stored at −20 °C. Tissues were homogenised and lipids extracted using the Folch technique [43]. Total cholesterol and triglycerides were then quantified using enzymatic, colorimetric assays described previously [44].

Statistical analyses

Data are presented as means ± SEM or as medians and ranges. Differences between two groups were assessed using *t* tests. Differences among three or more groups were evaluated by two-way analysis of variance followed by a Bonferroni multiple comparisons test. For variables with non-normal distribution, comparisons were performed using a nonparametric Mann–Whitney *U* test. Differences were accepted as statistically significant at $p < 0.05$. All *n* values represent the number of mice used in each group. For histological studies, at least two sections were examined of each tissue from each mouse.

Results

Age- and sex-dependent effects of loss of P2X7 receptor function on body mass and composition

At 9 months of age, male P2X7 KO mice appeared larger than male WT mice (Fig. 1a). WT and KO mice were sacrificed and weighed at 2, 6, 9 and 12 months of age. Interestingly, the total body weight of male KO mice was significantly greater than WT at 9 months of age (Fig. 1b, Supplementary Table S1). In contrast, there were no significant differences in the total body weight of female mice in any age group (Supplementary Table S2). The significant difference in body weight of male mice at 9 months of age was confirmed independently in a second cohort of mice (11 WT and 12 KO mice). When both cohorts were combined, the body weights of WT and KO mice were 39.5±1.7 and 48.9±1.3 g, respectively (means ± SEM, $n = 21$ and 22 mice, respectively, $p < 0.05$, *t* test).

To determine tissue changes underlying the greater body weight of KO mice, whole-body composition was analysed using micro-CT. Live mice were anaesthetised and scanned. Images were reconstructed at an isotropic voxel size of 150 or 154 μm and masses of adipose, lean and skeletal tissues determined using MicroView software and an in-house designed analysis program (Fig. 2a). Micro-CT confirmed greater total body mass in a third cohort of KO mice at 9 months of age and revealed significantly greater adipose tissue mass in these mice compared with WT controls (Fig. 2b, c). Using this approach, no significant differences in lean tissue mass, skeletal tissue mass, bone mineral content or bone mineral density were detected at any age (Fig. 2d–g).

Morphometric analysis of adipocytes from fat pads of WT and P2X7 KO mice

Since P2X7 is expressed in adipocytes [34] and the difference in total body mass was associated with a significant increase in adipose tissue, we examined the fat pads in WT and KO mice. Epididymal fat pads of WT and KO male mice (9 and 12 months of age) were isolated and weighed post-mortem. Fat pad mass was significantly greater in KO than in WT male mice at 9 months of age (Fig. 3a, b), with no significant difference observed at 12 months of age (Supplementary Table S1). In addition, no significant differences were observed in the mass of female parametrial fat pads (analogous to the epididymal fat pads in male mice) at either 9 or 12 months of age (Supplementary Table S2). Thus, these data show the same age- and sex-dependence as the differences in body weight and composition described above.

Histological assessments of epididymal fat pads in 9- and 12-month-old male mice revealed similar adipocyte morphology in WT and KO mice (Fig. 3c). Adipocyte size and density were determined by quantifying the largest diameter and counting the number of adipocytes per field of view (five fields of view analysed for two sections from each mouse fat pad). These parameters did not differ significantly in WT and KO mice of either age group (Fig. 3d, e). The similar size and

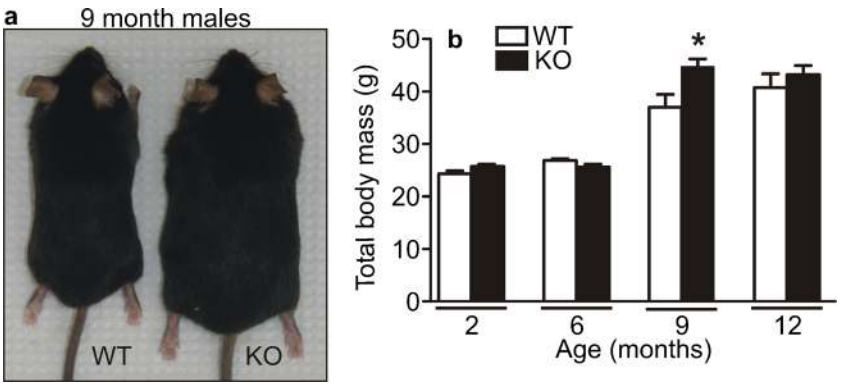

Fig. 1 Body weight of male wild-type (WT) and P2X7 knockout (KO) mice. **a** Image depicting the greater body size of a P2X7 KO male mouse in comparison to a WT male mouse at 9 months of age. **b** Two-, 6-, 9- and 12-month-old WT and KO mice were sacrificed and weighed to compare total body mass. Greater body weight was seen only at 9 months of age in KO mice compared with WT controls. Data are means ± SEM, $n = 10$ mice of each genotype and age. *Indicates significant difference between KO and WT ($p < 0.05$), determined by two-way analysis of variance and Bonferroni post hoc test

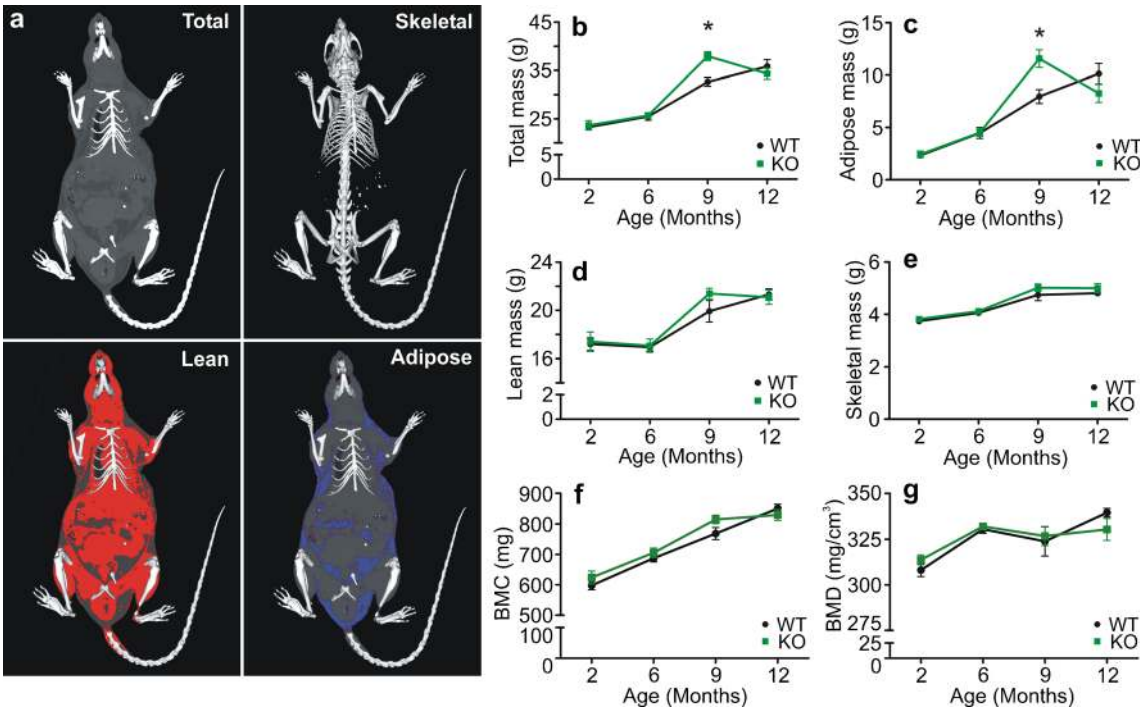

Fig. 2 Micro-CT analysis of whole-body composition of male WT and P2X7 KO mice. **a** *Top left panel* (Total) is a reconstructed micro-CT mid-coronal image of a live male 6-month-old WT mouse. Image was overlaid with the identified skeletal tissue (shown in white as a surface-rendered image in the *top right panel*). *Lower panels* are images of the same slice showing lean tissue in red and adipose tissue in blue. **b-g** Data are means ± SEM of the indicated parameters. Nine-month-old KO mice exhibited significantly greater total body mass and adipose tissue mass than WT controls. In contrast, lean tissue mass, skeletal mass, bone mineral content (BMC) and bone mineral density (BMD) were not significantly different at any age. *Indicates significant difference between KO and WT ($p<0.05$) at the same age, determined by two-way analysis of variance and Bonferroni post hoc test ($n=6$–8 mice of each genotype at each age)

density of adipocytes in WT and KO mice, together with the greater fat pad mass in 9-month-old male KO mice indicate that the difference in fat pad mass is due to adipocyte hyperplasia, rather than hypertrophy.

Histological differences in the kidneys of WT and KO mice

In addition to fat pads, several tissues from 2-, 9- and 12-month-old male and female mice were isolated post-mortem, weighed and assessed histologically. Histological differences were noted in specific tissues of older male mice using H&E staining. No differences were apparent in 2-month-old male mice or female mice at any age.

P2X7 is expressed in the collecting ducts of adult mouse kidney [45]. We found that, at both 9 and 12 months of age, kidney tissue exhibited spherical vacuole-like spaces (~3–12 μm in diameter; yellow arrowheads), which did not stain with H&E (Fig. 4a). There were markedly greater numbers of these spaces in male KO than in WT mice. We next examined tissues stained with osmium tetroxide, which specifically labels lipids and lipid-rich structures for optical microscopy [46]. A population of spherical structures stained positively with osmium tetroxide in kidney tissues only from KO mice (Fig. 4b, black stain), consistent with the presence of lipid droplets in some renal tubular epithelial cells. Image analysis revealed that osmium tetroxide staining was significantly greater in kidneys from KO than from WT mice (Fig. 4c). Based on size and shape, these osmium-stained structures appear to correspond to a subset of the spherical vacuole-like spaces identified in sections stained with H&E. Despite these histological alterations, there was no significant difference in the mass of the kidneys at any age in both males and females (Supplementary Tables S1 and S2).

Histological differences in the pancreases of WT and KO mice

In exocrine pancreas, P2X7 is expressed in ducts and may regulate secretion [27]. Pancreases were isolated from 2-, 9- and 12-month-old WT and KO mice. Striking histological differences were observed in male mice at 12 months of age; no differences were observed in younger mice or in female mice. Pancreatic tissues from 12-month-old male KO mice exhibited multiple large, membrane-bound structures (~10–30 μm in diameter), resembling adipocytes (Fig. 5a, b). The intracellular vacuole in these cells failed to stain with H&E. Staining with osmium tetroxide confirmed the presence of lipids (arrowheads) (Fig. 5c, d). These adipocytes were located in the exocrine pancreas predominantly among ducts and vasculature, as well as in boundaries between pancreatic lobes and sporadically among acini. No adipocytes were observed

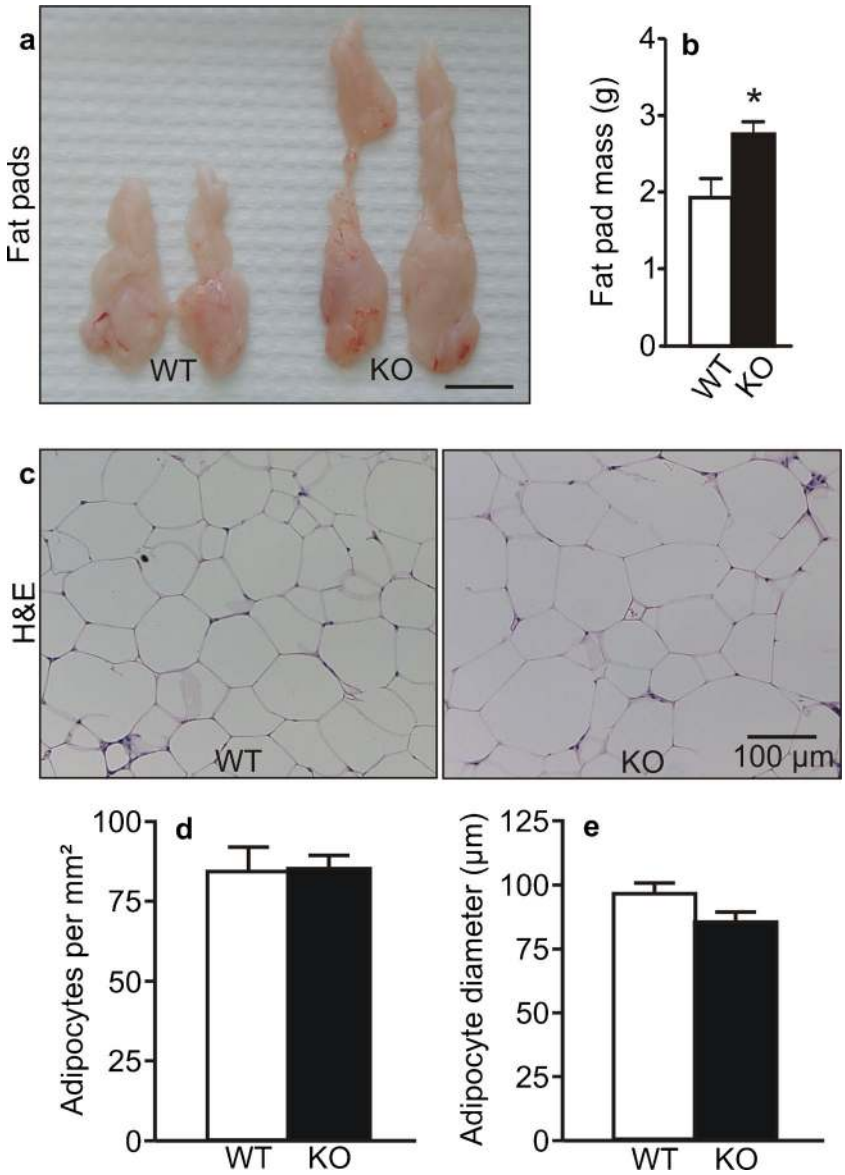

Fig. 3 Morphometric analysis of adipocytes in fat pads of male WT and P2X7 KO mice. Epididymal fat pads were isolated post-mortem. **a** Image depicting epididymal fat pads from a 9-month-old WT and KO mouse. Scale *bar* represents 1 cm. **b** Mass of epididymal fat pads was significantly greater in P2X7 KO than in WT male mice at 9 months of age. Data are means ± SEM, $n = 10$ mice of each genotype. Combined mass of right and left fat pads is reported. *Indicates significant difference between KO and WT ($p < 0.05$), determined by t test. **c** Representative histological sections of epididymal fat pads from 9-month-old male WT and P2X7 KO mice stained with H&E, with no marked differences in appearance. **d**, **e** Sections of fat pads from 9- and 12-month-old mice were analysed for adipocyte density and size. The number of adipocytes and largest diameter of each adipocyte in each field of view were measured. Data for 9-month-old mice are shown. For both 9- and 12-month-old mice, there was no significant difference between WT and KO in adipocyte density or size ($p > 0.05$, t test). Data are means ± SEM, $n = 5$ mice of each genotype and age with two sections and five fields of view per section analysed for each mouse

associated with pancreatic islets. By comparison, few adipocytes were seen in pancreatic tissues from age- and sex-matched WT mice. Quantification confirmed that osmium tetroxide staining was significantly greater in the pancreatic tissues of KO compared with WT mice (Fig. 5e). No differences were noted in the appearance of acini in WT and KO pancreases. There were also no significant differences between WT and KO in the mass of the pancreas at any age in male and female mice (Supplementary Tables S1 and S2).

Histological differences in the extraorbital lacrimal glands of WT and KO mice

Exocrine pancreas and extraorbital lacrimal glands are serous glands that exhibit similar histological appearances. P2X7 has been reported in both the acinar and ductal cells of rat lacrimal gland [47]. As observed for pancreas, we found a greater number of adipocytes in the extraorbital lacrimal glands of male mice at 12 months of age (Fig. 6), with no differences in younger or in female mice. These adipocytes were observed among the ducts and vasculature, as well as at the boundaries between lobes. In addition, small lipid droplets (~1 μm in diameter) accumulated in the basal aspect of lacrimal acinar cells to a much greater extent in KO than in WT mice (Fig. 6d, e). As in kidney and pancreas, osmium tetroxide staining was significantly greater in the extraorbital lacrimal glands of KO compared with WT mice (Fig. 6f). In males, the mass of the extraorbital lacrimal glands was significantly greater in KO than in WT mice at 2 months of age (Supplementary Table S1). However, there were no significant differences in older males or in females (Supplementary Table S2).

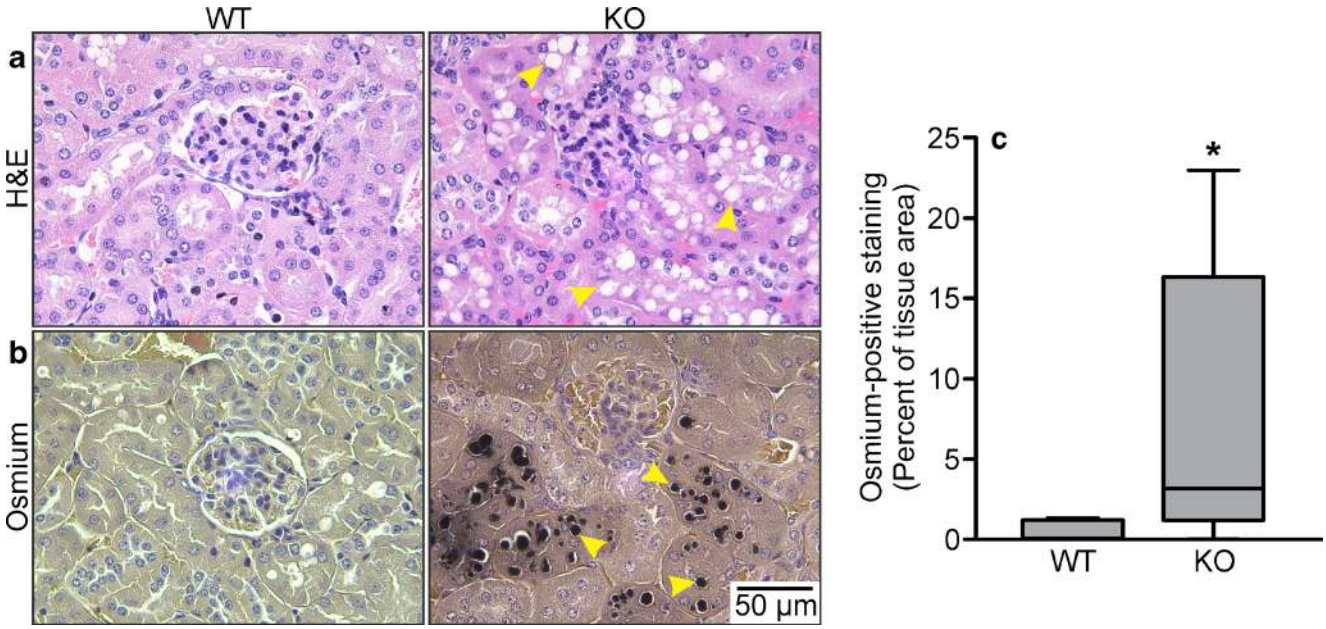

Fig. 4 Histology of kidneys in male WT and P2X7 KO mice. **a** Representative histological sections of cortico-medullary region of the kidney from 12-month-old male WT and P2X7 KO mice stained with H&E. At both 9 and 12 months of age, KO kidney exhibited multiple spherical structures (~3–12 μm in diameter, *yellow arrowheads*), which failed to stain with H&E. **b** Staining with osmium tetroxide revealed that these spherical structures were filled with lipid (*black*). Images shown are from 12-month-old male mice; similar results were found in 9-month-old male mice (not shown). Scale *bar* represents 50 μm for all images. Images are representative of 8–11 male mice of each genotype and age (9 and 12 months). **c** For 12-month-old mice, the area that stained positively with osmium tetroxide was determined using image analysis and expressed as a percentage of the total tissue area. Data are medians and interquartile ranges (IQR, *boxes*) with *whiskers* representing the 10th and 90th percentiles; $n=5$ mice of each genotype with two sections per mouse. At least two fields of view per section were analysed. *Indicates a significant difference between KO and WT ($p<0.05$), determined by one-tailed Mann–Whitney *U* test

Histological differences in the salivary glands of WT and KO mice

P2X7 expression has been reported previously in both ductal and acinar cells of mouse submandibular gland [48, 49]. Interestingly, in our study, the submandibular salivary gland displayed multiple spherical structures that did not stain with H&E (Fig. 7a). Like the kidney tissues, a greater number of these structures were observed in glandular tissue from older male KO mice than from WT mice. However, in contrast to the tissues described above, these spherical structures in the submandibular gland did not stain with osmium tetroxide (Fig. 7b), revealing the absence of lipid. In addition, these structures appeared to be located centrally within acini of the submandibular gland but were absent in the adjacent sublingual gland. Moreover, there were no significant differences in the mass of the salivary glands at any age in both males and females (Supplementary Tables S1 and S2).

Histology of spleen and other tissues of interest in WT and KO mice

P2X7 is highly expressed in cells of the immune system and therefore in organs such as the spleen [33]. Spleens were isolated post-mortem, weighed and assessed histologically at 9 and 12 months of age. H&E revealed greater basophilic staining coupled with megakaryocyte hyperplasia in male KO compared with WT mice at 12 months of age (Fig. 8a). These histological differences were accompanied by significantly greater mass of the spleen (Fig. 8b). Osmium tetroxide did not reveal lipid staining in the spleen (not shown).

Several other tissues were isolated post-mortem and assessed by histology. Livers and hearts from male KO mice had significantly larger masses than WT at 9 months of age, a difference not seen at 12 months of age. No histological differences between WT and KO were apparent in these tissues or in skeletal muscle at either age. No other histological or weight differences were seen in males (Supplementary Table S1). In females, no significant differences were seen in the mass of any of the tissues examined (Supplementary Table S2). Furthermore, no histological differences were seen in any female tissues at any age (data not shown).

Food consumption, blood plasma chemistry and tissue lipid analyses

To assess whether the phenotype seen in older male mice was the result of differences in diet, food consumption was measured by weighing food once weekly. No significant differences in average daily food consumption were seen between

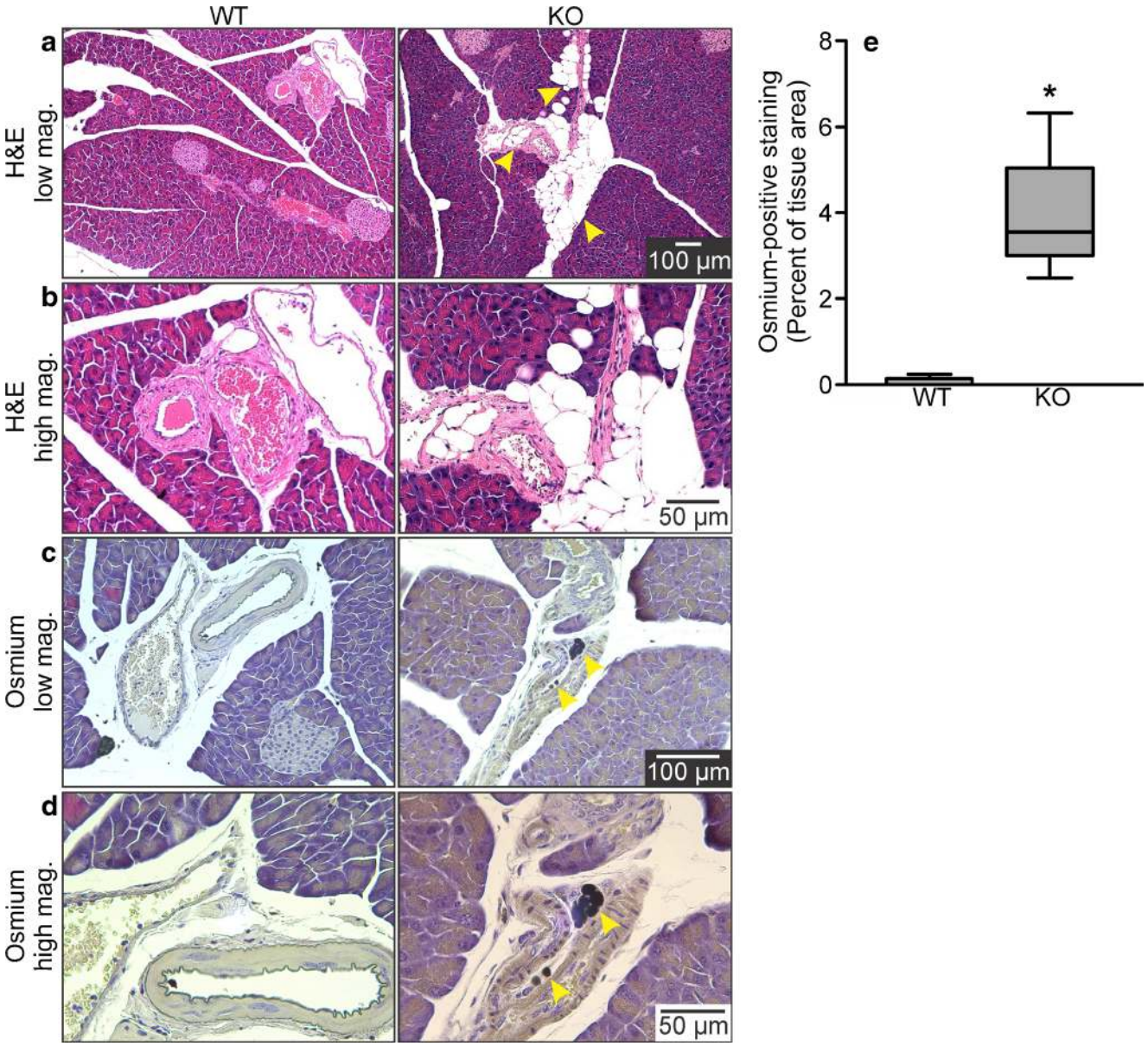

Fig. 5 Histology of pancreas in male WT and P2X7 KO mice. Images are representative histological sections at low magnification (**a** and **c**), with higher magnification images from the same fields shown in **b** and **d**. **a**, **b** Representative histological sections of pancreas from 12-month-old male WT and P2X7 KO mice stained with H&E. KO pancreas exhibited multiple large membrane-bound spherical structures (~10–30 µm in diameter, *yellow arrowheads*), which failed to stain with H&E, resembling adipocytes. These structures were located predominantly among ducts and vasculature, as well as in boundaries between pancreatic lobes. **c**, **d** Staining with osmium tetroxide confirmed the identity of these cells as adipocytes (*yellow arrowheads*). Images are representative of ten male mice of each genotype. **e** The area that stained positively with osmium tetroxide was determined using image analysis and expressed as a percentage of the total tissue area. Data are medians and IQR (*boxes*) with *whiskers* representing the 10th and 90th percentiles; $n = 5$ mice of each genotype with two sections per mouse. At least two fields of view per section were analysed. *Indicates a significant difference between KO and WT ($p < 0.05$), determined by one-tailed Mann–Whitney *U* test

male WT and KO mice at any age (Fig. 9), suggesting that the phenotype may be due to metabolic differences.

To investigate the metabolic phenotype, blood plasma samples were obtained by cardiac puncture and assayed for glucose, triglyceride and total cholesterol. In comparison to WT, male KO mice had significantly reduced plasma cholesterol levels at both 9 and 12 months of age. No significant differences in plasma triglyceride or glucose levels were seen at either age for WT and KO mice (Table 1). Furthermore, no significant differences in any plasma parameters were seen in female WT and KO mice at 9 and 12 months of age (Supplementary Table S3). Selected tissues were isolated post-mortem to determine whether histological changes were accompanied by changes in tissue levels of triglycerides or total cholesterol. KO mouse heart tissue had significantly reduced tissue cholesterol levels in comparison to WT controls at 9 months of

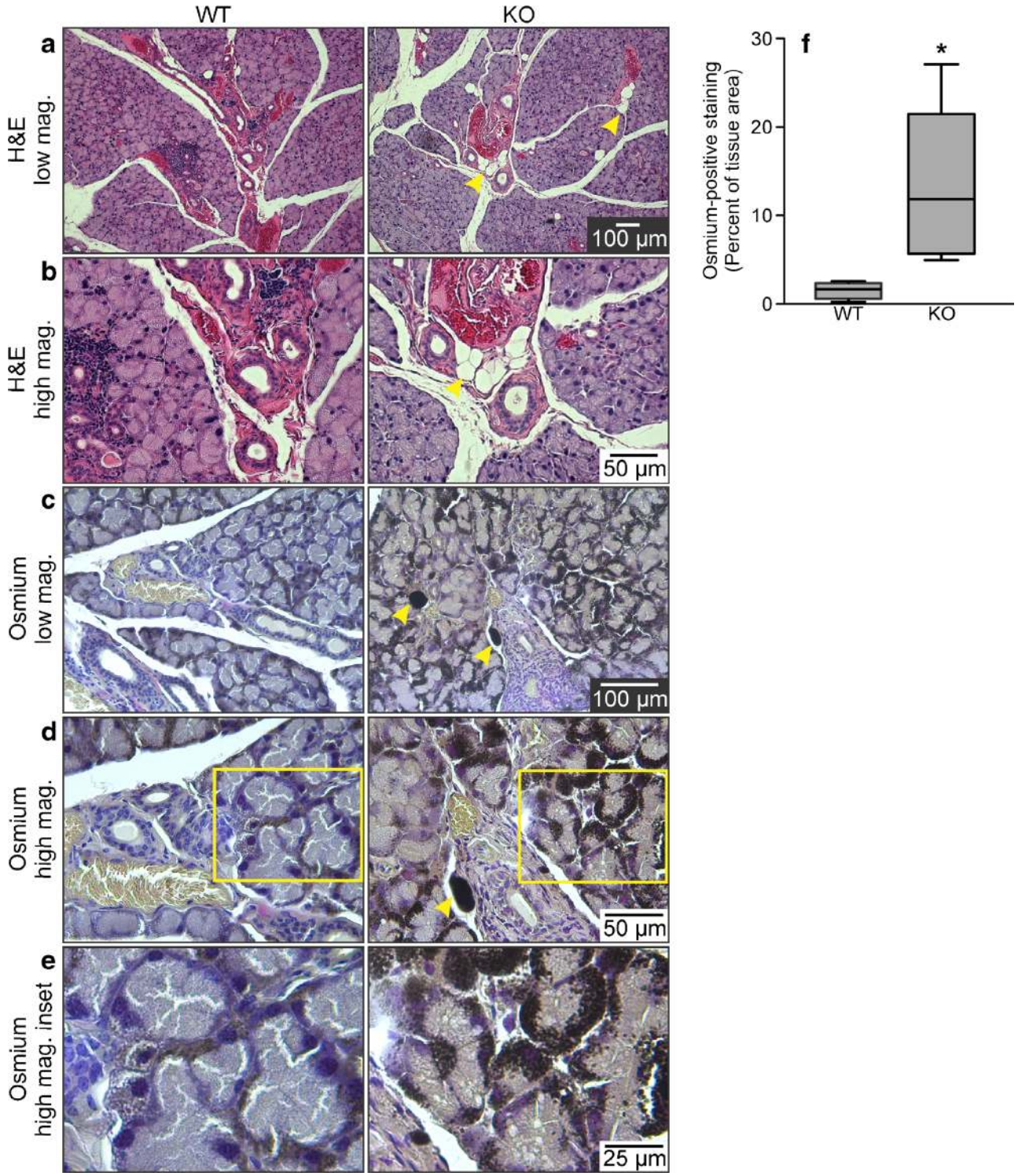

Fig. 6 Histology of extraorbital lacrimal glands in male WT and P2X7 KO mice. Images are representative histological sections at low magnification (**a** and **c**), with higher magnification images from the same fields shown in **b**, **d** and **e**. **a**, **b** Representative histological sections of extraorbital lacrimal glands from 12-month-old male WT and P2X7 KO mice stained with H&E. Similar to pancreas, adipocyte-like cells (*yellow arrowheads*) were observed among ducts and vasculature, as well as in boundaries between lobes in glands from KO mice. **c**, **d** Osmium tetroxide staining confirmed the presence of adipocytes in the KO tissues. **e** Higher magnification images of regions outlined by yellow rectangles in **d**. These images reveal markedly greater accumulation of small lipid droplets in the basal cytoplasm of acinar cells in the KO mice. Images are representative of ten male mice of each genotype. **f** The area that stained positively with osmium tetroxide was determined using image analysis and expressed as a percentage of the total tissue area. Data are medians and IQR (*boxes*) with *whiskers* representing the 10th and 90th percentiles; $n = 5$ mice of each genotype with two sections per mouse. At least two fields of view per section were analysed. *Indicates a significant difference between KO and WT ($p < 0.05$), determined by one-tailed Mann–Whitney *U* test

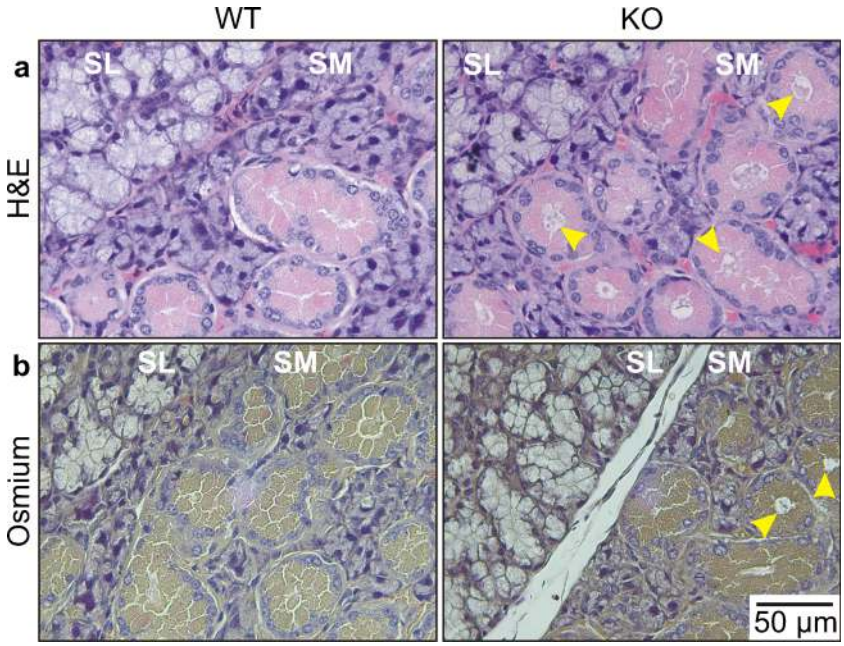

Fig. 7 Histology of salivary glands in male WT and P2X7 KO mice. **a** Representative histological sections of salivary glands from 12-month-old male WT and P2X7 KO mice stained with H&E (*SM*: submandibular gland, *SL*: sublingual gland). At both 9 and 12 months of age, multiple spherical structures, which failed to stain with H&E (*yellow arrowheads*), were observed in the submandibular but not sublingual gland. **b** Staining with osmium tetroxide revealed that these spherical structures did not contain lipid (images shown are from 12-month-old male mice). Scale *bar* represents 50 μm for all images. Images are representative of 8–11 male mice of each genotype and age (9 and 12 months)

age whereas there were no significant differences in triglyceride or cholesterol levels in other tissues (Supplementary Table S4).

Discussion

The P2X7 receptor serves a number of important functions in multiple tissues throughout the body. Previous in vitro studies have shown that P2X7 suppresses expression of adipocyte differentiation markers [13] and acts through phospholipases and sphingomyelinases to generate bioactive lipid signalling molecules [50]. Here, we report abnormal adipocyte and lipid accumulation in mice lacking functional P2X7, pointing to a generalised role for P2X7 in regulating lipid storage and metabolism in vivo.

We used the Pfizer KO mouse in which there is global disruption of P2X7 function [25, 39]. This mouse model has been studied extensively; however, most studies have focused on the phenotype of younger animals. It has previously been reported that the Pfizer KO mouse displays no gross phenotypic differences at early ages [19, 33, 51]. In the present study, we allowed these mice to age, which revealed an unexpected increase in body mass due to greater lipid accumulation in older male KO mice. Previous characterisation of the femurs and tibias of older Pfizer KO mice revealed diminished periosteal bone formation and excessive trabecular bone resorption [19]. In the present study, we did not detect any difference in skeletal mass at the whole-body level, perhaps indicating regional effects of P2X7 disruption.

We observed that fat pad mass was greater in KO than in WT male mice at 9 months of age. An increase in adipose tissue mass can result from greater adipocyte size (hypertrophy), greater adipocyte cell number (hyperplasia), or both [52]. Previous studies have shown that both visceral and subcutaneous adipocytes express P2X7 receptors [34, 53]. Adipocyte size and density were similar in WT and KO, indicating that the increase in mass was due to adipocyte hyperplasia. Adipocyte number is determined both by the recruitment and

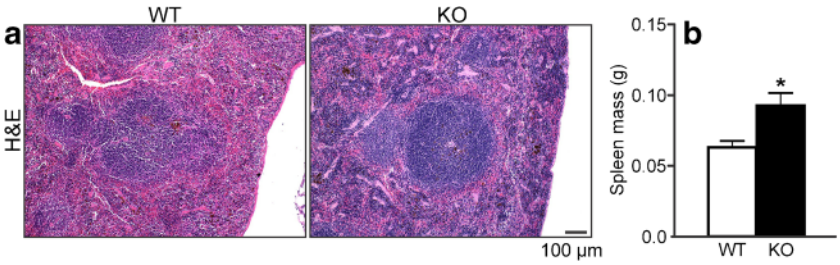

Fig. 8 Histology of spleen in male WT and P2X7 KO mice. **a** Representative histological sections of spleen from 12-month-old male WT and P2X7 KO mice stained with H&E. Images revealed greater basophilic staining coupled with megakaryocyte hyperplasia in the KO compared with the WT spleen. No differences between WT and KO were observed in spleen sections stained with osmium tetroxide (not shown). **b** The mass of the spleen was significantly greater in KO than in WT at 12 months of age only. Data are means ± SEM, $n = 10$ mice of each genotype (*$p < 0.05$, *t* test)

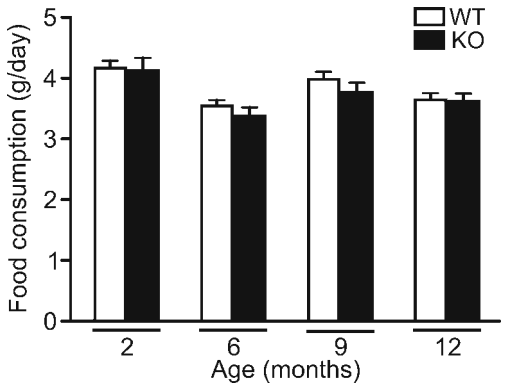

Fig. 9 Food consumption by male WT and P2X7 KO mice. Food consumption was measured by weighing food once weekly. No significant differences were seen at any age between the WT and KO mice. Data are the mean consumption per day and are expressed as means ± SEM, $p > 0.05$, determined by two-way analysis of variance and Bonferroni post hoc test, $n \geq 6$ mice of each genotype and age

differentiation of stem cells into mature adipocytes and by adipocyte apoptosis [54]. Therefore, our results suggest that loss of P2X7 may decrease apoptosis of mature adipocytes or increase adipogenesis from mesenchymal stem cells.

Mesenchymal stem cells are widely distributed in connective tissues such as bone marrow, as well as in the perivascular niche [55]. These cells are capable of differentiating into multiple lineages including fibroblasts, chondrocytes, osteoblasts and adipocytes. Moreover, human mesenchymal stem cells have been shown to express several P2 receptors including P2X7 by both RT-PCR and immunoblotting [56]. In addition, we have shown previously that cultures of bone cells from Pfizer P2X7 KO mice display greater expression of adipogenic markers compared to WT cells [13]. Thus, P2X7 may suppress adipocyte differentiation from mesenchymal stem cells. In this regard, when mesenchymal stem cells are induced to differentiate into adipocytes, exogenous ATP reduces the formation of lipid droplets and suppresses adipogenic differentiation [56]. Taken together, these in vitro results support our in vivo findings of greater numbers of adipocytes in P2X7 KO mice.

In the present study, the observed distribution of adipocytes in adipose tissues and ectopically in perivascular regions of the KO mice corresponds to locations where mesenchymal stem cells are known to reside. Previous studies have shown that mesenchymal stem cells exist in both lacrimal glands [57] and pancreas, specifically in ductal regions [58]. Thus, it is possible that loss of P2X7 enhances the differentiation of mesenchymal progenitor cells toward the adipocyte lineage, resulting in increased adipocyte numbers in periductal regions of the pancreas and lacrimal glands. In future studies, lineage tracing could be used to determine the commitment of mesenchymal progenitors to adipocytes, shedding light on the role of P2X7 in adipogenesis.

Recent work has shown that P2X7 regulates cellular metabolism. Grol and coworkers showed that activation of P2X7 leads to a dramatic, glucose-dependent increase in metabolic acid production by osteoblasts [31]. In addition, work from another lab has shown that heterologous expression of P2X7 in vitro leads to upregulation of glycolytic enzymes and an increase in lactate production [32]. Thus, overall energy expenditure may be less in mice lacking functional P2X7 receptors, resulting in increased accumulation of fat as the animals age. It is also possible that P2X7 receptors have direct effects on lipid metabolism. In this regard, several studies have shown that P2X7 couples to activation of phospholipases in various cell types [13, 37, 50, 59]. Thus, loss of P2X7 function in cells that normally express this receptor may disrupt lipid metabolism leading to the eventual accumulation of lipid droplets in the cytosol.

Novak and coworkers have shown previously that Pfizer KO mice display abnormal exocrine secretion from the pancreas and lacrimal glands [60]. Pancreatic secretion was significantly reduced in KO mice, whereas tear production was increased. Interestingly, the secretory phenotype was affected by the sex of the animal, with males more dependent on P2X7 expression, as observed for ectopic lipid deposition in the present study and skeletal remodeling in a previous study [19]. This sexual dimorphism may reflect interactions between estrogen and P2X7 signaling. In this regard, it has been shown previously that 17β-estradiol inhibits P2X7-mediated currents through a non-genomic mechanism [61].

In the present study, accumulation of lipid droplets was also observed in the renal tubular epithelium. Previous reports have shown that, in healthy mice, P2X7 is expressed in the renal collecting duct but not in the glomeruli or other tubules [62]. The function of P2X7 in collecting duct remains poorly understood. A previous study reported no abnormalities in renal morphology or histology in a different P2X7 KO mouse model (6- to 8-week-old female mice) [51]. In the present

Table 1 Blood plasma cholesterol, triglyceride and glucose levels (in millimoles per litre) in male wild-type (WT) and P2X7 knockout (KO) mice

Parameter	9 months		12 months	
	WT	KO	WT	KO
Cholesterol	3.83±0.27	2.91±0.10*	3.34±0.10	2.77±0.21*
Triglycerides	0.72±0.05	1.03±0.15	0.89±0.12	0.70±0.07
Glucose	11.42±0.77	10.69±0.82	11.36±0.73	12.31±0.56

Glucose, triglycerides and total cholesterol (millimoles per litre) were measured in blood plasma samples obtained by cardiac puncture. In comparison to WT, KO mice had significantly reduced plasma cholesterol levels both at 9 and 12 months of age. No significant differences in plasma triglyceride or glucose levels were seen between WT and KO mice at either age. Data are means ± SEM, $*p < 0.05$ compared with corresponding WT based on unpaired two-tailed t test, $n = 9$ mice of each genotype and age

study, lipid droplets were observed only in older male mice, perhaps explaining the lack of phenotype in the earlier study.

In our study, no histological differences were observed in liver, heart, skeletal muscle or Harderian glands. Although it has been reported that P2X7 is expressed in hepatocytes, and cardiac and skeletal myocytes [53, 63, 64], there was no apparent accumulation of lipid in these cells. Therefore, absence of P2X7 alone is not sufficient to trigger lipid abnormalities in all tissues.

Analysis of blood plasma revealed significantly reduced levels of total cholesterol in the male KO mice in older age groups. In contrast to humans, mice carry cholesterol mainly in the form of high-density lipoprotein (HDL) [65–67]. On the other hand, fasting blood glucose concentrations were not significantly different between WT and KO mice of all age groups and sexes. Therefore, it was unlikely that the heavier KO males were diabetic. Furthermore, assessment of food intake in our study revealed no significant differences between WT and KO mice at any age. Additionally, others have reported no differences in spontaneous locomotor activity of P2X7 WT and KO mice [68]. Therefore, the changes in adiposity in older males are likely due to metabolic dysregulation. The present study reveals that P2X7 KO mice exhibit some of the characteristics of metabolic syndrome, including increased central adiposity, reduced levels of HDL and the deposition of ectopic lipids in lean tissues.

We found that loss of P2X7 had noticeable effects on body weight and adiposity only in older animals. These findings are consistent with other studies showing no differences in body weight between P2X7 KO and WT mice at younger ages, even when fed a high-fat diet [33, 69]. Aging itself is known to be associated with metabolic dysfunction including alterations in glucose and fatty acid metabolism, and redox homeostasis [70]. Thus, it is possible that the additional metabolic impairment arising from loss of P2X7 results in a phenotype only when combined with age-related changes in metabolism. Alternatively, it is conceivable that loss of P2X7 affects younger mice but results in such gradual lipid accumulation that it manifests only in older animals. Interestingly, total mass and fat pad mass were significantly greater in KO than in WT mice at 9 months of age, but there were no significant differences in 12-month-old animals. Thus, it is possible that loss of P2X7 function accelerates age-related changes in body composition.

In summary, we have shown that male mice lacking functional P2X7 receptors develop ectopic lipid accumulations as they age. Our study reveals that P2X7 receptors play a generalised role in regulating lipid storage and metabolism in vivo. Further research is required to elucidate the role of P2X7 in regulating the differentiation of adipocytes from mesenchymal stem cells. As well, our findings provide additional impetus to probe the emerging roles of P2X7 in the control of energy and lipid metabolism.

Acknowledgements This work was funded by the Canadian Institutes of Health Research (CIHR) [grant number 102542]. KLB and AX were supported in part by the Joint Motion Program—A CIHR Training Program in Musculoskeletal Health Research and Leadership. MWG was supported by a CIHR Frederick Banting and Charles Best Canada Graduate Scholarship Doctoral Award. DWH holds the Dr. Sandy Kirkley Chair in Musculoskeletal Research at The University of Western Ontario. We thank Dr. Nattapon Panupinthu for performing preliminary studies, Linda Jackson and Tom Chrones for assistance with histology, Vasek Pitelka for aiding with animal anaesthesia, Dr. Joseph Umoh for micro-CT scanning, Drs. Tom Daley and Ian Welch for advice on histopathology, Cindy Sawyez and Brian Sutherland for assistance with biochemical analyses and Dr. Nica Borradaile for helpful comments.

Conflict of interest The authors have no conflicts of interest to declare.

References

1. Dixon JB (2010) The effect of obesity on health outcomes. Mol Cell Endocrinol 316:104–108
2. Hassan M, Latif N, Yacoub M (2012) Adipose tissue: friend or foe? Nat Rev Cardiol 9:689–702
3. Dulloo AG, Montani JP (2012) Body composition, inflammation and thermogenesis in pathways to obesity and the metabolic syndrome: an overview. Obes Rev 13(Suppl 2):1–5
4. Shuldiner AR, Yang R, Gong DW (2001) Resistin, obesity and insulin resistance—the emerging role of the adipocyte as an endocrine organ. N Engl J Med 345:1345–1346
5. Ducy P, Amling M, Takeda S, Priemel M, Schilling AF, Beil FT, Shen J, Vinson C, Rueger JM, Karsenty G (2000) Leptin inhibits bone formation through a hypothalamic relay: a central control of bone mass. Cell 100:197–207
6. Ferron M, Wei J, Yoshizawa T, Del Fattore A, DePinho RA, Teti A, Ducy P, Karsenty G (2010) Insulin signaling in osteoblasts integrates bone remodeling and energy metabolism. Cell 142:296–308
7. Jacobi D, Stanya KJ, Lee CH (2012) Adipose tissue signaling by nuclear receptors in metabolic complications of obesity. Adipocyte 1: 4–12
8. Suganami T, Tanaka M, Ogawa Y (2012) Adipose tissue inflammation and ectopic lipid accumulation. Endocr J 59:849–857
9. Kopecky J, Rossmeisl M, Flachs P, Brauner P, Sponarova J, Matejkova O, Prazak T, Ruzickova J, Bardova K, Kuda O (2004) Energy metabolism of adipose tissue—physiological aspects and target in obesity treatment. Physiol Res 53(Suppl 1):S225–S232
10. Lee NK, Sowa H, Hinoi E, Ferron M, Ahn JD, Confavreux C, Dacquin R, Mee PJ, McKee MD, Jung DY, Zhang Z, Kim JK, Mauvais-Jarvis F, Ducy P, Karsenty G (2007) Endocrine regulation of energy metabolism by the skeleton. Cell 130:456–469
11. Medina-Gomez G (2012) Mitochondria and endocrine function of adipose tissue. Best Pract Res Clin Endocrinol Metab 26:791–804
12. Burnstock G (2007) Physiology and pathophysiology of purinergic neurotransmission. Physiol Rev 87:659–797
13. Panupinthu N, Rogers JT, Zhao L, Solano-Flores LP, Possmayer F, Sims SM, Dixon SJ (2008) P2X7 receptors on osteoblasts couple to production of lysophosphatidic acid: a signaling axis promoting osteogenesis. J Cell Biol 181:859–871
14. Hughes JP, Hatcher JP, Chessell IP (2007) The role of $P2X_7$ in pain and inflammation. Purinergic Signal 3:163–169
15. Sorge RE, Trang T, Dorfman R, Smith SB, Beggs S, Ritchie J, Austin JS, Zaykin DV, Vander Meulen H, Costigan M, Herbert TA, Yarkoni-Abitbul M, Tichauer D, Livneh J, Gershon E, Zheng M, Tan K, John SL, Slade GD, Jordan J, Woolf CJ, Peltz G, Maixner W, Diatchenko

L, Seltzer Z, Salter MW, Mogil JS (2012) Genetically determined P2X7 receptor pore formation regulates variability in chronic pain sensitivity. Nat Med 18:595–599
16. Coutinho-Silva R, Persechini PM, Bisaggio RD, Perfettini JL, Neto AC, Kanellopoulos JM, Motta-Ly I, Dautry-Varsat A, Ojcius DM (1999) P_{2Z}/$P2X_7$ receptor-dependent apoptosis of dendritic cells. Am J Physiol 276:C1139–C1147
17. Gu BJ, Saunders BM, Petrou S, Wiley JS (2011) $P2X_7$ is a scavenger receptor for apoptotic cells in the absence of its ligand, extracellular ATP. J Immunol 187:2365–2375
18. Surprenant A, Rassendren F, Kawashima E, North RA, Buell G (1996) The cytolytic P_{2Z} receptor for extracellular ATP identified as a P_{2X} receptor ($P2X_7$). Science 272:735–738
19. Ke HZ, Qi H, Weidema AF, Zhang Q, Panupinthu N, Crawford DT, Grasser WA, Paralkar VM, Li M, Audoly LP, Gabel CA, Jee WS, Dixon SJ, Sims SM, Thompson DD (2003) Deletion of the $P2X_7$ nucleotide receptor reveals its regulatory roles in bone formation and resorption. Mol Endocrinol 17:1356–1367
20. Li JLD, Ke HZ, Duncan RL, Turner CH (2005) The $P2X_7$ nucleotide receptor mediates skeletal mechanotransduction. J Biol Chem 280: 42952–42959
21. Grol MW, Panupinthu N, Korcok J, Sims SM, Dixon SJ (2009) Expression, signaling, and function of P2X7 receptors in bone. Purinergic Signal 5:205–221
22. Dubyak GR (2012) P2X7 receptor regulation of non-classical secretion from immune effector cells. Cell Microbiol 14:1697–1706
23. Miller CM, Boulter NR, Fuller SJ, Zakrzewski AM, Lees MP, Saunders BM, Wiley JS, Smith NC (2011) The role of the $P2X_7$ receptor in infectious diseases. PLoS Pathog 7:e1002212
24. Sakowicz-Burkiewicz M, Kocbuch K, Grden M, Maciejewska I, Szutowicz A, Pawelczyk T (2013) High glucose concentration impairs ATP outflow and immunoglobulin production by human peripheral B lymphocytes: involvement of P2X7 receptor. Immunobiology 218:591–601
25. Solle M, Labasi J, Perregaux DG, Stam E, Petrushova N, Koller BH, Griffiths RJ, Gabel CA (2001) Altered cytokine production in mice lacking $P2X_7$ receptors. J Biol Chem 276:125–132
26. Burnstock G, Novak I (2013) Purinergic signalling and diabetes. Purinergic Signal 9:307–324
27. Novak I (2008) Purinergic receptors in the endocrine and exocrine pancreas. Purinergic Signal 4:237–253
28. Ducy P, Zhang R, Geoffroy V, Ridall AL, Karsenty G (1997) Osf2/Cbfa1: a transcriptional activator of osteoblast differentiation. Cell 89:747–754
29. Rosen ED, Walkey CJ, Puigserver P, Spiegelman BM (2000) Transcriptional regulation of adipogenesis. Genes Dev 14:1293–1307
30. Muruganandan S, Roman AA, Sinal CJ (2009) Adipocyte differentiation of bone marrow-derived mesenchymal stem cells: cross talk with the osteoblastogenic program. Cell Mol Life Sci 66:236–253
31. Grol MW, Zelner I, Dixon SJ (2012) $P2X_7$-mediated calcium influx triggers a sustained, PI3K-dependent increase in metabolic acid production by osteoblast-like cells. Am J Physiol Endocrinol Metab 302: E561–E575
32. Amoroso F, Falzoni S, Adinolfi E, Ferrari D, Di Virgilio F (2012) The P2X7 receptor is a key modulator of aerobic glycolysis. Cell Death Dis 3:e370
33. Sun S, Xia S, Ji Y, Kersten S, Qi L (2012) The ATP-$P2X_7$ signaling axis is dispensable for obesity-associated inflammasome activation in adipose tissue. Diabetes 61:1471–1478
34. Madec S, Rossi C, Chiarugi M, Santini E, Salvati A, Ferrannini E, Solini A (2011) Adipocyte $P2X_7$ receptors expression: a role in modulating inflammatory response in subjects with metabolic syndrome? Atherosclerosis 219:552–558
35. Sim JA, Young MT, Sung HY, North RA, Surprenant A (2004) Reanalysis of $P2X_7$ receptor expression in rodent brain. J Neurosci 24:6307–6314
36. Labasi JM, Petrushova N, Donovan C, McCurdy S, Lira P, Payette MM, Brissette W, Wicks JR, Audoly L, Gabel CA (2002) Absence of the $P2X_7$ receptor alters leukocyte function and attenuates an inflammatory response. J Immunol 168:6436–6445
37. Panupinthu N, Zhao L, Possmayer F, Ke HZ, Sims SM, Dixon SJ (2007) P2X7 nucleotide receptors mediate blebbing in osteoblasts through a pathway involving lysophosphatidic acid. J Biol Chem 282:3403–3412
38. Naemsch LN, Dixon SJ, Sims SM (2001) Activity-dependent development of $P2X_7$ current and Ca^{2+} entry in rabbit osteoclasts. J Biol Chem 276:39107–39114
39. Masin M, Young C, Lim K, Barnes SJ, Xu XJ, Marschall V, Brutkowski W, Mooney ER, Gorecki DC, Murrell-Lagnado R (2012) Expression, assembly and function of novel C-terminal truncated variants of the mouse P2X7 receptor: re-evaluation of P2X7 knockouts. Br J Pharmacol 165:978–993
40. Granton PV, Norley CJ, Umoh J, Turley EA, Frier BC, Noble EG, Holdsworth DW (2010) Rapid in vivo whole body composition of rats using cone beam μCT. J Appl Physiol 109:1162–1169
41. Gulam M, Thornton MM, Hodsman AB, Holdsworth DW (2000) Bone mineral measurement of phalanges: comparison of radiographic absorptiometry and area dual X-ray absorptiometry. Radiology 216:586–591
42. Carson FL (1996) Histotechnology: a self-instructional text. American Society for Clinical Pathology, Chicago
43. Folch J, Lees M, Sloane Stanley GH (1957) A simple method for the isolation and purification of total lipids from animal tissues. J Biol Chem 226:497–509
44. Burnett JR, Wilcox LJ, Telford DE, Kleinstiver SJ, Barrett PH, Newton RS, Huff MW (1997) Inhibition of HMG-CoA reductase by atorvastatin decreases both VLDL and LDL apolipoprotein B production in miniature pigs. Arterioscler Thromb Vasc Biol 17: 2589–2600
45. Hillman KA, Burnstock G, Unwin RJ (2005) The $P2X_7$ ATP receptor in the kidney: a matter of life or death? Nephron Exp Nephrol 101: e24–e30
46. Belazi D, Sole-Domenech S, Johansson B, Schalling M, Sjovall P (2009) Chemical analysis of osmium tetroxide staining in adipose tissue using imaging ToF-SIMS. Histochem Cell Biol 132:105–115
47. Hodges RR, Vrouvlianis J, Shatos MA, Dartt DA (2009) Characterization of $P2X_7$ purinergic receptors and their function in rat lacrimal gland. Invest Ophthalmol Vis Sci 50:5681–5689
48. Pochet S, Garcia-Marcos M, Seil M, Otto A, Marino A, Dehaye JP (2007) Contribution of two ionotropic purinergic receptors to ATP responses in submandibular gland ductal cells. Cell Signal 19:2155–2164
49. Nakamoto T, Brown DA, Catalan MA, Gonzalez-Begne M, Romanenko VG, Melvin JE (2009) Purinergic $P2X_7$ receptors mediate ATP-induced saliva secretion by the mouse submandibular gland. J Biol Chem 284:4815–4822
50. Costa-Junior HM, Marques-da-Silva C, Vieira FS, Moncao-Ribeiro LC, Coutinho-Silva R (2011) Lipid metabolism modulation by the P2X7 receptor in the immune system and during the course of infection: new insights into the old view. Purinergic Signal 7:381–392
51. Taylor SR, Turner CM, Elliott JI, McDaid J, Hewitt R, Smith J, Pickering MC, Whitehouse DL, Cook HT, Burnstock G, Pusey CD, Unwin RJ, Tam FW (2009) $P2X_7$ deficiency attenuates renal injury in experimental glomerulonephritis. J Am Soc Nephrol 20:1275–1281
52. Bjorntorp P (1991) Adipose tissue distribution and function. Int J Obes 15(Suppl 2):67–81

53. Volonte C, Amadio S, D'Ambrosi N, Colpi M, Burnstock G (2006) P2 receptor web: complexity and fine-tuning. Pharmacol Ther 112: 264–280
54. Drolet R, Richard C, Sniderman AD, Mailloux J, Fortier M, Huot C, Rheaume C, Tchernof A (2008) Hypertrophy and hyperplasia of abdominal adipose tissues in women. Int J Obes (Lond) 32:283–291
55. Bouacida A, Rosset P, Trichet V, Guilloton F, Espagnolle N, Cordonier T, Heymann D, Layrolle P, Sensebe L, Deschaseaux F (2012) Pericyte-like progenitors show high immaturity and engraftment potential as compared with mesenchymal stem cells. PLoS One 7:e48648
56. Zippel N, Limbach CA, Ratajski N, Urban C, Luparello C, Pansky A, Kassack MU, Tobiasch E (2012) Purinergic receptors influence the differentiation of human mesenchymal stem cells. Stem Cells Dev 21:884–900
57. You S, Kublin CL, Avidan O, Miyasaki D, Zoukhri D (2011) Isolation and propagation of mesenchymal stem cells from the lacrimal gland. Invest Ophthalmol Vis Sci 52:2087–2094
58. Rovira M, Scott SG, Liss AS, Jensen J, Thayer SP, Leach SD (2010) Isolation and characterization of centroacinar/terminal ductal progenitor cells in adult mouse pancreas. Proc Natl Acad Sci U S A 107:75–80
59. Le Stunff H, Auger R, Kanellopoulos J, Raymond MN (2004) The Pro-451 to Leu polymorphism within the C-terminal tail of P2X7 receptor impairs cell death but not phospholipase D activation in murine thymocytes. J Biol Chem 279:16918–16926
60. Novak I, Jans IM, Wohlfahrt L (2010) Effect of $P2X_7$ receptor knockout on exocrine secretion of pancreas, salivary glands and lacrimal glands. J Physiol 588:3615–3627
61. Cario-Toumaniantz C, Loirand G, Ferrier L, Pacaud P (1998) Non-genomic inhibition of human $P2X_7$ purinoceptor by 17β-oestradiol. J Physiol 508:659–666
62. Hillman KA, Johnson TM, Winyard PJ, Burnstock G, Unwin RJ, Woolf AS (2002) $P2X_7$ receptors are expressed during mouse nephrogenesis and in collecting duct cysts of the cpk/cpk mouse. Exp Nephrol 10:34–42
63. Emmett DS, Feranchak A, Kilic G, Puljak L, Miller B, Dolovcak S, McWilliams R, Doctor RB, Fitz JG (2008) Characterization of ionotrophic purinergic receptors in hepatocytes. Hepatology 47:698–705
64. Young CN, Brutkowski W, Lien CF, Arkle S, Lochmuller H, Zablocki K, Gorecki DC (2012) P2X7 purinoceptor alterations in dystrophic *mdx* mouse muscles: relationship to pathology and potential target for treatment. J Cell Mol Med 16:1026–1037
65. Daugherty A (2002) Mouse models of atherosclerosis. Am J Med Sci 323:3–10
66. Zadelaar S, Kleemann R, Verschuren L, de Vries-Van der Weij J, van der Hoorn J, Princen HM, Kooistra T (2007) Mouse models for atherosclerosis and pharmaceutical modifiers. Arterioscler Thromb Vasc Biol 27:1706–1721
67. Getz GS, Reardon CA (2012) Animal models of atherosclerosis. Arterioscler Thromb Vasc Biol 32:1104–1115
68. Basso AM, Bratcher NA, Harris RR, Jarvis MF, Decker MW, Rueter LE (2009) Behavioral profile of $P2X_7$ receptor knockout mice in animal models of depression and anxiety: relevance for neuropsychiatric disorders. Behav Brain Res 198:83–90
69. Glas R, Sauter NS, Schulthess FT, Shu L, Oberholzer J, Maedler K (2009) Purinergic $P2X_7$ receptors regulate secretion of interleukin-1 receptor antagonist and beta cell function and survival. Diabetologia 52:1579–1588
70. Houtkooper RH, Argmann C, Houten SM, Canto C, Jeninga EH, Andreux PA, Thomas C, Doenlen R, Schoonjans K, Auwerx J (2011) The metabolic footprint of aging in mice. Sci Rep 1:134